Answers to Anonymous Referee #3

We thank the anonymous referee #3 for his/her constructive comments and suggestions that certainly have improved the manuscript significantly. We revised the manuscript according to his/her comments and the comments of anonymous referees #1 and #2. In the following,

- *referee's comments are given in italic*,
- our answers are outlined in normal format, and
- **textual changes in the manuscript are given in bold format**.

We would like inform the anonymous referee #3 about the following changes:

1. Driven by the specific comment (SC) #18 of anonymous referee #3 (SC3.18), we decided to drop scenario S4 from the analysis. The difference between the sub-adiabatic model (S3) and the modified one (S4) is that the latter accounts for the depletion of the liquid water content due to entrainment, precipitation, and freezing drops. Consequently, we wanted to check whether S4 captures better the vertical stratification of the modeled low-level clouds and, accordingly, if it approximates the CREs of the reference simulation with better accuracy. Since S4 does not provide any further insight, we now have decided to drop this scenario. However, we do confirm that, by considering all the case days in the analysis, we came to the same conclusions as for 3 June. As a confirmation, we updated the Tables and attached them at the end of this document. The referee is referred to Tables R1–R3.

2. In all scenarios, we decided to drop sub-case d, which employs two fixed values for the droplet number concentration representing the two modes in the corresponding histogram for 3 June 2016. This scenario separates clouds into a cluster with low/high clouds. Considering the vertical variability of the droplet number concentration, the latter clustering will link low clouds (within the boundary layer) with high N_d and, accordingly, high clouds with lower N_d values. Thus, for all scenarios, employing such values for N_d are able to approximate the reference radiative transfer simulation very well. Only the radiative transfer simulation that is supplied by the droplet number concentration weighted over the cloud geometrical extent, i.e., N_int (sub-case b) leads to smaller differences when compared to the reference simulation. However, we do confirm that, by considering all the case days into the analysis, we came to the same conclusions as for 3 June. Note that, for the latter case, the clustering was conducted on the mean N_int over all case days. As a confirmation, we updated the Tables and attached them at the end of this document. The referee is referred to Tables R1–R3.

3. We decided to add a new scenario as a replacement of sub-case d, whereby radiative transfer simulations are conducted for a mean vertical profile of the droplet number concentration over all case days. Tables R9–R11 summarize the new results. In brief, this scenario is considered as an improvement compared to the clustering case. The following parts were included within the text:

   Section 5.1.2: **Last but not least, by replacing the vertical profile of N_d by the**

mean profile of N_d over all case days (see Fig. 2), emulates the cloud radiative effects of the reference simulation quite well. Accordingly, scenario S4 slightly undersimates the mean SW CREs, with an mean error up to $-3.16\,\mathrm{W\,m^{-2}}$ and a RMSE up to $17.2\,\mathrm{W\,m^{-2}}$ for both BOA and TOA. In fact, this scenario outperforms the rest scenarios (S1–S3), except from the sub-case b (N_{int}) in all scenarios. For an illustration of the excellent linear correlation between the reference simulation and S4 by means of a bivariate kernel density (BKD) plot, the reader is referred to Fig. B1 in Appendix B. One can see that the CREs computed by these scenarios are in a very good agreement almost everywhere except towards larger values of the CREs in case of the SW radiation, with Pearson correlations larger than 0.977 for both BOA and TOA.

Section 6: **By employing a more representative profile for the N_d, i.e., a mean vertical profile of N_d over all case days leads to a rather good approximation; the RMSE is below $17.2\,\mathrm{W\,m^{-2}}$. This points to the need to better account for prognostic N_d calculations.**

Appendix B: **In sect. 5.1.2, by conducting idealized radiative transfer simulations, we estimated the impact of the representation of cloud properties in ICON-LEM on the cloud radiative effects (CREs). Special emphasis was given on identifying the droplet number concentration (N_d), which approximates the microphysical and radiative properties of low-level clouds as simulated by ICON-LEM (reference scenario). A radiative transfer simulation, which employs a mean vertical profile of N_d over all the case days (scenario S4), approximates the CREs of the reference scenario quite well. Figure B1 depicts the excellent linear correlation between the reference simulation and S4 by means of a bivariate kernel density (BKD)**.

4. Following the general comment of anonymous referee #2 for shortening the manuscript given the redundancy of many of the results shown in this study and his/her relevant specific comments (SC), i.e., (SC2.12) and (SC2.25):

   - We decided to drop Fig. B1. Figure B1 illustrates the bivariate kernel density (BKD) between the cloud optical thickness and the liquid water path on a logarithmic scale. Considering the comprehensive explanation given in Sect. 3.3.1, we decided that this illustration did not provide any additional information.
   - Figures 6 and 7 have been revised. Now, they illustrate results only for TOA (see Figs R2 and R3).
   - We now focus only on the rotational component analysis. The mention of the principal component analysis have been significantly reduced. In addition, we removed the relevant information from Table 3. For the updated version of the Table, the referees are referred to Table R5. Additionally, we replaced Figure 5 by Table R4. This table lists the contribution of each rotational component to the total variance.

Answers to general comments (GC) from referee #3 (GC3)

(GC3.1) *The robustness of the obtained results, such as principal components of cloud properties and their relationship with the CRE, should be discussed. These results are obtained only from the one-day data. However, the daily variation is large as shown in Table. 1, although the authors claim that the day has similar properties to the six-day average.*

We revised our manuscript according to the comments of anonymous referee #3 and the comments of anonymous referees #1 and #2. We further extended our analysis over all case days to improve the robustness of our results. Now, sections 3.2 and 5 outline our findings for all case days.

Answers to specific comments (SC) from referee #3 (SC3)

(SC3.1) *Order of diagrams in Figures*

The order of sub-figures has been revised.

(SC3.2) *Significant figures of values.*

The number of significant figures of values has been revised.

(SC3.3) *Brief descriptions of the model and configurations of the experiment are necessary, such as kind of governing equations, vertical levels, and calculation domains.*

We revised the description of ICON-LEM (Section 2.1) according to the anonymous referee 3 and the specific comment (SC3) of anonymous referee 1:.

The ICON unified modeling framework was co-developed by the German meteorological service (DWD) and the Max Planck institute for meteorology (MPI-M) in order to support climate research and weather forecasting. Within the HD(CP)2 project, ICON was further extended towards large eddy simulations with realistic topography **and** open boundary conditions. This resulted in ICON-LEM **deployed in restricted areas that are centered on Germany and the Tropical Atlantic [1]. The equations utilized by the model are based on the prognostic variables given by Gassmann and Herzog [2]. These variables comprise the horizontal and vertical velocity components, the density of moist air, the virtual potential temperature, and the mass and number densities of traces, e.g., specific humidity, liquid water, and different ice hydrometeors. A comprehensive description of the model and its governing equations is found in Dipankar et al. [3] and Wan et al., [4].** Concerning turbulence parameterization, the three-dimensional Smagorinsky scheme is employed [3]. The activation of cloud condensation nuclei (CCN) is based on the parameterization of Seifert and Beheng [5] and modified in order to account for the consumption of CCNs due to their activation into cloud droplets. The CCN concentration is then parameterized following the pressure profile and the vertical velocity [6].

Simulations are carried out for three different domains with 624 m, 312 m, and 156 m

horizontal resolution. The model domains consist of 150 vertical levels, with resolutions ranging from ∼25 m to 70 m within the boundary layer, and from 70 m to 355 m further up until the top of the domain at 21 km. For each of the aforementioned grids, data is stored as one-dimensional (1D) profiles every 10 sec, two-(2D), and 3D snapshots [1]. The model yields output on each of the aforementioned grids with the data stored as one-dimensional (1D) profiles, two-(2D), and 3D snapshots [1]. In case of the 3D output, the simulation data is interpolated from the original grids (e.g., 156 m) to a 1 km grid, the 3D coarse data, and 300 m grid, the so-called HOPE data. The latter output has been created for the purpose of model evaluation with ground-based observations from the HD(CP)^2 Observational Prototype Experiment (HOPE) that took place near Jülich [7]**and is limited to a domain size of about ∼45 km^2. Note here that for the 2D and 3D output, data is stored at day- and night-time frequency. Day-time frequency begins at 06:00 UTC and lasts until 00:00 UTC, while night-time starts at midnight and lasts until 06:00 UTC. The 2D data is stored with a day-time and night-time frequency of 10 sec and 5 min, respectively. The 3D coarse data have day-time frequency of 10 min (1 hour at night-time). In this study, the 3D HOPE data has been used that is stored only at a day-time frequency of 15 min.**

(SC3.4) *Equation 15. The fact 9/5 seems to be 3/2. The power of (18w4 fad ad) is not 1/6 but -1/6.*

The referee is correct. This section has been revised following also the specific comment #2 of the anonymous referee #1 (SC1.2):

P6 L24: **while the factor** $2/3$ **is a scale factor resulting from the constant liquid water content and effective radius with height [8]**.

P7 L21: **Compared to Eq. (7), Eq. (10) leads to a factor of** $5/9$**, meaning that the sub-adiabatic liquid water path is** $5/6$ **times the one of the vertically homogeneous model [9]**.

P8 L11: **For vertically constant** q_{L} **and** r_{eff}**, this can be interpreted as the cloud optical thickness coming from the vertical homogeneous model (see Eq. 7). According to the sub-adiabatic cloud model, the cloud optical thickness is linked to the liquid water path and the effective radius [10],**

$$\tau = \frac{9}{5}\frac{Q_{\mathrm{L}}}{\rho_{\mathrm{w}} \cdot r_{\mathrm{eff}}}$$

Alternatively, substituting r_{eff} **from Eq. (13) in Eq. (15), the cloud optical thickness is given by,...**

(SC3.5) *P9 L18: A close relation between the effective radius and the droplet number concentration exist. Why does the effective radius have a single-mode distribution in spite of the bimodal distribution of the droplet number concentration?*

The effective radius is defined as the ratio of the third to the second moments of the droplet size distribution and the second moment of the size distribution is closely related to the liquid water content. Accordingly, the two modes of N_{d} do not need to be at two different size regimes in r_{eff}.

(SC3.6) *P9 L18: "exist" -¿ exists.*

Corrected.

(SC3.7) *Figure 2 and Figure 3 (b) Both diagrams show the distribution of the Nd, the magnitude of the median is quite different. What makes such a big difference?*

Figure 2 shows the histogram as a box-whisker plot of the droplet number concentration for each model level. On the other hand, Fig. 3 depicts the mean profile of N_{d} normalized over the cloud geometrical extent, illustrating the vertical change in N_{d} within individual clouds. The aforementioned normalization is the reason of the differences between the two figures. As we aforementioned, we further extended the analysis over all case days. Thus, fig. (2) and fig. (3) have been revised (see Fig. R1 and Fig. R2).

(SC3.8) *Section 3.3.1: There is a large relationship between Q_{L} and fad, and then this analysis has multicollinearity problem. Therefore, the amount obtained must be much interpolated more carefully. Furthermore, I do not agree that the is proportional to $Q_{\mathrm{L}}^{5/6}$, since Eq. (15) has f_{ad}.*

We acknowledge referee's concerns with respect to our multicollinearity analysis. However, we respectfully disagree on this point. In this section, we tried to predict the cloud optical thickness derived from the output of ICON-LEM (by using Eq. 14), via employing the relevant equation suggested by the sub-adiabatic model, i.e., Eq. (15). In the analysis, results from all case days has been considered. By employing the sub-adiabatic model, i.e., model $Y_4(Q_{\mathrm{L}}, f_{\mathrm{ad}}, N_{\mathrm{int}})$, we managed to approximate the cloud optical thickness quite well. In fact, Y_4 explains 99.9% of the variance in cloud optical thickness with a root mean square error of 0.027. In addition, we found only a weak correlation between the liquid water path and the sub-adiabatic factor (Pearson correlation of 0.28), in contrast to the very strong correlation between the cloud optical thickness and the liquid water path (Pearson correlation of 0.99). The referee is referred to Figure 4 in section 4.

However, we did revise section 3.1.1, in order to avoid any confusion. The following parts have been included:

P13 L2: **With this intention, an effort has been conducted to predict the cloud optical thickness derived from Eq. (14) by employing the sub-adiabatic model and Eq. (15).**

Caption of Table 2: Prediction of cloud optical thickness by ordinary least squares regression method:

P13 L20: **In fact, model $Y_4(Q_{\mathrm{L}}, f_{\mathrm{ad}}, N_{\mathrm{int}})$ supports the applicability of the sub-adiabatic model since it is able to approximate the cloud optical thickness with high accuracy** (RMSE = 0.027)

(SC3.9) *P17 L19: resulting in a net cooling. There exists large uncertainty, and I wondered if the negative value has statistical significance.*

We acknowledge the referee's concerns with regard to the uncertainty in the resulting cloud ra-

diative effects. However, low-level clouds tend to be rather warm and, hence, having a generally small influence on the TOA lowngwave radiation. In contrast, they are characterized by a large albedo, leading to an overall net cooling effect. The latter net cooling effect has been reported by several observational studies [11, 12, 13, 14, 15, 16].

(SC3.10) *P18 L1, Table 6 lists the mean CREs between... It should be "Table 6 lists the difference of the mean CREs between...". The same corrections are necessary for the following sentences.*

We thank the referee for highlighting the mistake. The text has been revised.

(SC3.11) *P18 L8. For a given liquid water path, the smaller... Check if it is grammatically correct.*

We double-checked the sentence and think it is correct.

(SC3.12) *P18 L16, a Pearson correlation of 0.950 (0.928) is yielded. The values are 0.952 (0.930) in Table 6.*

We thank the referee for highlighting the mismatches between the table and the text. Nevertheless, we now extended the analysis over all days and, thus, tables and related text have been revised.

(SC3.13) *P18 L19, a Pearson correlation of 0.995. The value is 0.996 in Table 6.*

The same as in (SC3.12).

(SC3.14) *P18 L19, and P20 L13, no suprise considering surprise*

The text has been revised as follows:

The latter can be explained by the way the droplet number concentration is derived (see Eq. 4)...

(SC3.15) *P18 L25, of about -6.52 Wm^{-2} with a RMSE of 10.4 Wm^{-2} for b and -9.31 Wm^{-2} with a RMSE of 19.4 Wm^{-2} for d The sign of -6.52 and -9.31 is different from that in Table 6. The mismatch is also in the number of -0.11 and -3.64 at Page 19 Line 1.*

We thank the referee for highlighting the mismatches between the table and the text. We have now extended the analysis over all days and, thus, tables and related text have been revised.

(SC3.16) *Table 6. The names of Scen. are wrong.*

The referee is correct. However, we now have decided to replace the sub-scenario (d, clusters) with a new scenario 4, whereby we employ the mean droplet number concentration profile over all days. Accordingly, Table 6 has been revised. The referee is referred to the section **General changes**.

(SC3.17) *P19 L3, For instance, in case of the adiabatic scenarios... the sub-adiabatic.*

The text is revised accordingly.

(SC3.18) *P19 L7, slightly larger scatter is found for S4 as compared to S3. Why is the result of S4 worth than that of S3?*

The difference between the sub-adiabatic model (S3) and the modified one (S4) is that the latter accounts for the depletion of the liquid water content due to entrainment, precipitation, and freezing drops. Consequently, we wanted to check whether it captures better the vertical stratification of the modeled low-level clouds and, accordingly, if it approximates the CREs of the reference simulation with better accuracy. Since S4 does not provide any further insight, we now have decided to drop this scenario. However, we do confirm that, by considering all the case days into the analysis, we came to the same conclusions as for 3 June. As a confirmation, we updated the Tables and attached them at the end of this document. The referee is referred to Tables R1–R3.

(SC3.19) *P20 L7: -0.76. It has different significant figures from that in Table 7. Same for 0.21 at P20 L13.*

We thank the referee for highlighting the mismatches. We have now extended the analysis over all days and, thus, tables and related text have been revised.

(SC3.20) *Logarithmic axis is preferred. The saturation may not be found in the logarithmic plot.*

We acknowledge the referee's suggestion for the logarithmic axis. However, we respectfully disagree on this point. Firstly, we would like to highlight that, in the SW radiation, an excellent monotonic relation is found between the CREs and cloud optical thickness, liquid water path, and cloud geometrical extent for both BOA and TOA. Secondly, the SW CRE is negative and the logarithm of a negative number is undefined. Even if we take the absolute value of the CRE, we still see the monotonic relation, but, it is less pronounced.

(SC3.21) *P21 L3, e.g., Fig. 6 panels (a) or (b) with Fig. 8 panel (b) Fig. 8 panel (a).*

We thank the referee for pointing to the mistake. Nevertheless, we now have reduced the amount of plots. Following the general comment of the anonymous referee #2, we now illustrate only the results for TOA (see Figs. R3 and R4).

(SC3.22) *P21 L3, The resulting Spearman and Pearson correlations larger than 0.96 and 0.91, respectively. The values seem to be 0.816 and 0.914.*

The correct panels of Fig. 8 are (a) and (d). Accordingly, the Spearman correlation is 0.96 and 0.935. Nevertheless, we now extended the analysis over all case days and, thus, the correlations have slightly changed.

(SC3.23) *P21 L14, with Spearman and Pearson correlations above -0.796 and -0.82, respectively. The values should be -0.820 and -0.796. The author should mention that these values are only for high values of the droplet number concentration.*

The referee is correct. However, we now have decided to replace the sub-scenario (d, clusters) with a new scenario 4, whereby we employ the mean droplet number concentration profile over all case days. For details with respect to the relevant changes, the referee is referred to section **General changes**.

List of Figures

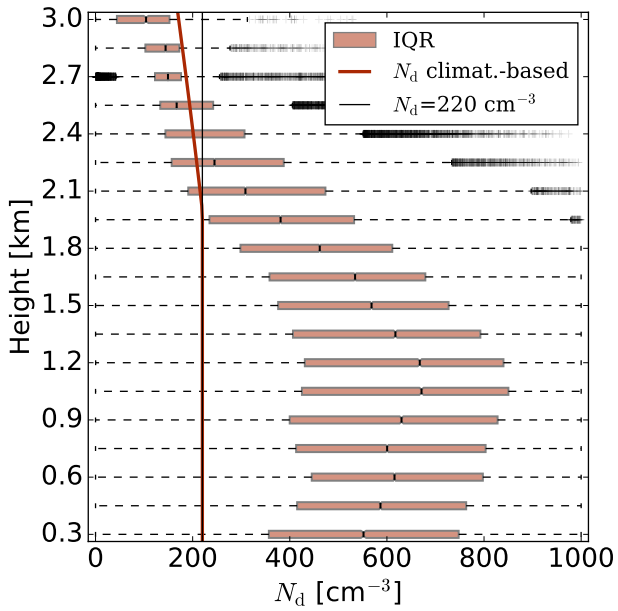

Figure R1: Box-whisker plot of the droplet number concentration for all the case days on average, describing the histograms of N_d simulated for different model levels by the double moment scheme of ICON-LEM. Boxes illustrate interquartile range (IQR), dark red line denotes the vertical N_d profile in case of the droplet number concentration employed in coarse climate models (climat.-based) and the thin black line demonstrates the constant N_d profile of 220 cm^{-3}.

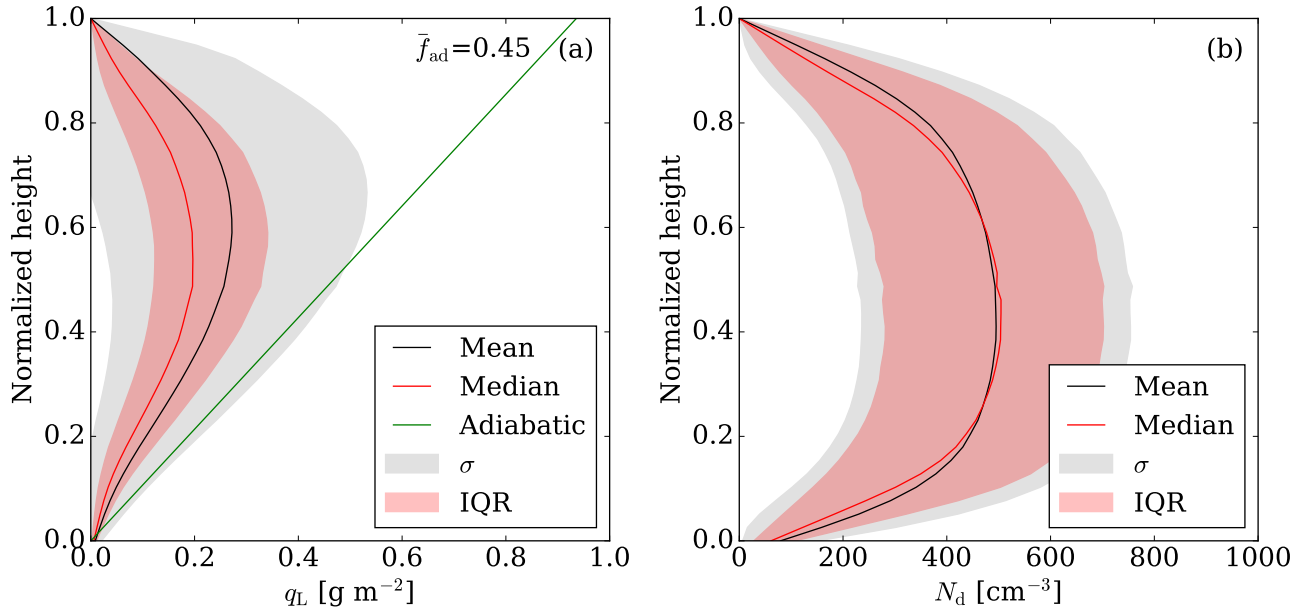

Figure R2: ICON-LEM simulated mean (a) q_L and (b) N_d profiles for all the case days on average. Profiles are normalized over height from the CBH to the CTH. Black lines denote the mean, red solid lines the median, gray shaded areas the standard deviation, red shaded areas the interquartile range (IQR), and the green solid line outline the mean adiabatic q_L profile characterized by a mean adiabatic fraction ($\bar{f}_{ad}$) of 0.45.

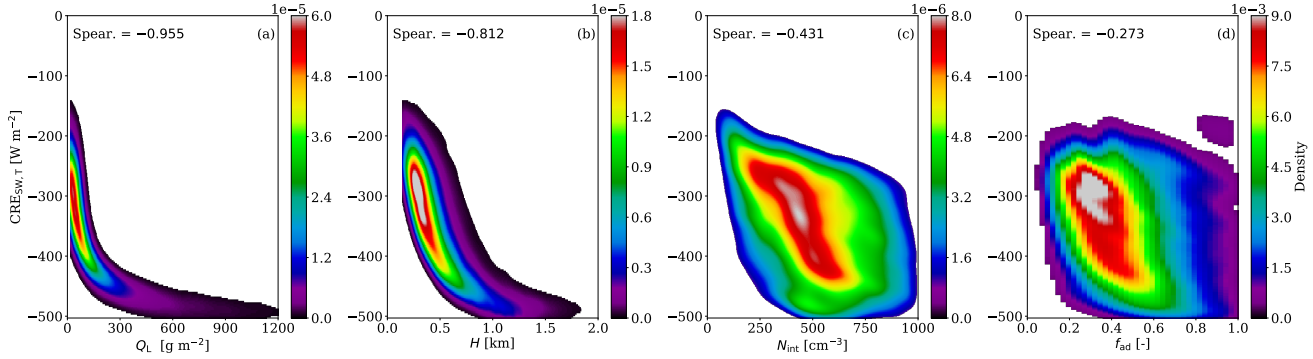

Figure R3: Bivariate kernel density (BKD) between the reference simulation (Ref.) and the cloud properties that are essential for the derivation of the cloud optical thickness that is one of the fundamental properties describing the SW cloud radiative effect. Panels illustrate the BKD between the $CRE_{SW,T}$ and (a) Q_L, (b) H, (c) N_{int}, and (d) f_{ad}. The corresponding Spearman (Spear.) correlations are highlighted.

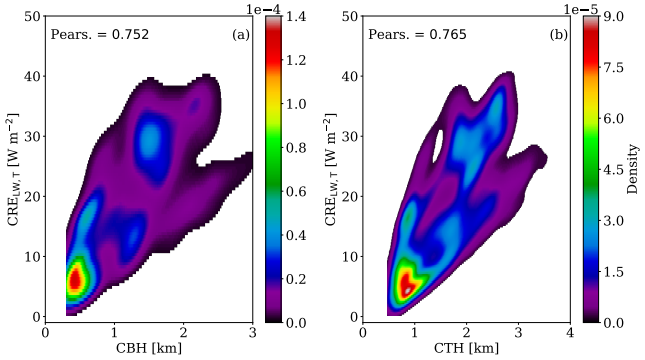

Figure R4: Bivariate kernel density (BKD) between the reference simulation (Ref.) and the cloud properties describing the LW cloud radiative effect at the BOA and (a) CBH and (b) CTH. The corresponding Pearson (Pears.) correlations are highlighted.

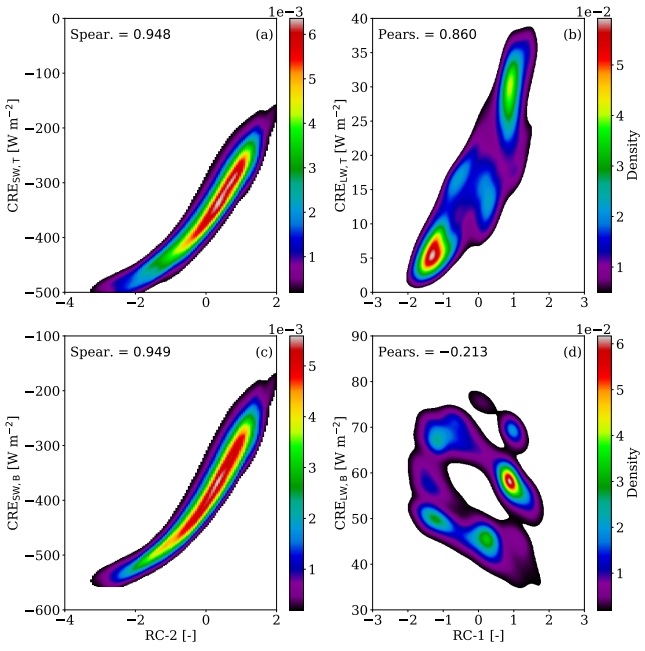

Figure R5: For the reference simulation (Ref.), bivariate kernel density (BKD) between CRE_{SW} and the second rotational component (RC-2) at (a) TOA, (c) BOA and between CRE_{LW} and the first rotational component (RC-1) at (b) TOA, (d) BOA. The corresponding Spearman (Spear.) and Pearson (Pears.) correlations are highlighted for the SW and LW radiation, respectively.

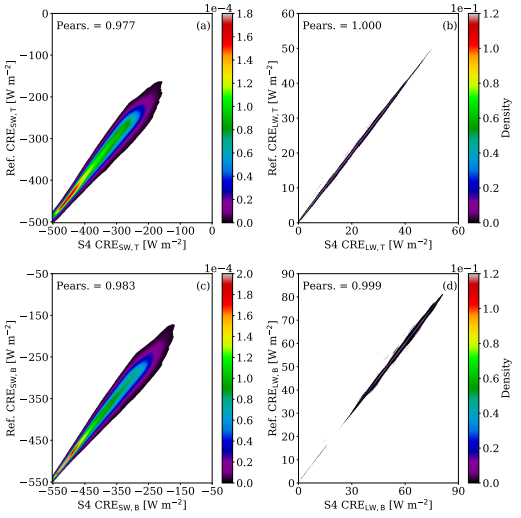

Figure R6: Bivariate kernel density (BKD) between the reference simulation (Ref.) and the scenario that employs the mean vertical N_{d} profile (S4). For the CREs, BKD are presented for the SW radiation at the TOA (a) and BOA (c), and for the LW radiation at the TOA (b) and BOA (d). The corresponding Pearson (Pears.) correlations are highlighted.

List of Tables

Table R1: Mean CRE ($\mathrm{W\,m^{-2}}$) for the SW radiation. Results are given as differences between the new scenario minus the reference simulation (Δ). The root mean square error (RMSE) in $\mathrm{W\,m^{-2}}$ and the Pearson (Pears.) correlation between the new scenarios and the reference simulation are also given.

Scen.	$\mathrm{CRE_{SW,B}}$			$\mathrm{CRE_{SW,T}}$		
	Δ	RMSE	Pears.	Δ	RMSE	Pears.
S1a	−39.2	46.4	0.960	−40.1	47.0	0.952
S1b	−7.04	11.7	0.995	−6.53	11.7	0.994
S1c	−2.59	23.4	0.964	−1.86	24.3	0.951
S1d	−6.57	17.6	0.982	−5.99	18.0	0.977
S2a	−26.1	39.2	0.943	−27.1	39.8	0.930
S2b	7.74	14.2	0.991	8.19	13.6	0.990
S2c	12.9	32.4	0.943	13.7	33.6	0.921
S2d	8.53	22.6	0.971	9.10	22.9	0.964
S3a	−31.1	41.4	0.950	−32.9	42.9	0.937
S3b	1.47	10.6	0.993	1.17	10.0	0.992
S3c	6.59	27.7	0.953	6.55	29.0	0.934
S3d	2.29	19.1	0.976	2.09	19.5	0.969
S4a	−28.7	40.1	0.947	−30.3	41.4	0.934
S4b	4.97	11.7	0.993	4.80	11.1	0.992
S4c	10.1	29.9	0.949	10.2	31.2	0.928
S4d	5.72	20.4	0.975	5.67	20.8	0.967

Table R2: Mean CRE ($\mathrm{W\,m^{-2}}$) for the LW radiation. Results are given as differences between the new scenario minus the reference simulation (Δ). The root mean square error (RMSE) in $\mathrm{W\,m^{-2}}$ and the Pearson (Pears.) correlation between the new scenarios and the reference simulation are also given.

Scen.	$\mathrm{CRE_{LW,B}}$			$\mathrm{CRE_{LW,T}}$		
	Δ	RMSE	Pears.	Δ	RMSE	Pears.
S1a	−0.11	0.48	0.999	−0.04	0.19	1.000
S1b	−0.05	0.40	0.999	−0.03	0.18	1.000
S1c	−0.01	0.50	0.999	−0.01	0.22	1.000
S1d	−0.04	0.45	0.999	−0.02	0.21	1.000
S2a	0.40	0.79	0.998	0.23	0.51	0.999
S2b	0.51	0.82	0.998	0.27	0.53	0.999
S2c	0.55	0.85	0.998	0.29	0.54	0.999
S2d	0.52	0.83	0.998	0.28	0.53	0.999
S3a	−0.05	0.74	0.997	0.33	0.64	0.999
S3b	−0.01	0.73	0.997	0.36	0.65	0.999
S3c	0.02	0.83	0.996	0.37	0.68	0.998
S3d	0.00	0.75	0.997	0.37	0.65	0.999
S4a	0.11	0.71	0.997	0.31	0.59	0.999
S4b	0.21	0.70	0.998	0.34	0.60	0.999
S4c	0.24	0.76	0.997	0.37	0.62	0.999
S4d	0.22	0.72	0.997	0.35	0.61	0.999

Table R3: Correlations between the cloud radiative effects and the cloud properties for the two major clusters characterized by low N_{int} values (L) and high N_{int} values (H). For the SW (LW) radiation, results are presented in case of the Spearman (Pearson) correlation.

Properties	$\mathrm{CRE_{SW,B}}$		$\mathrm{CRE_{SW,T}}$		$\mathrm{CRE_{LW,B}}$		$\mathrm{CRE_{LW,T}}$	
	L	H	L	H	L	H	L	H
Q_{L}	−0.935	−0.988	−0.930	−0.978	−0.016	−0.309	0.216	0.303
τ	−0.992	−0.994	−0.983	−0.986	0.028	−0.324	0.195	0.291
N_{int}	−0.446	−0.128	−0.410	−0.105	0.419	0.202	-0.259	−0.067
r_{int}	−0.343	−0.867	−0.353	−0.854	−0.311	−0.365	0.323	0.268
CBH	0.143	−0.213	−0.057	−0.292	−0.311	−0.239	0.752	0.786
CTH	−0.122	−0.604	−0.201	−0.663	−0.302	−0.376	0.783	0.717
H	−0.776	−0.921	−0.787	−0.925	−0.024	−0.386	0.217	0.300
f_{ad}	−0.126	−0.271	−0.129	−0.256	−0.003	0.144	0.215	0.194

Table R4: Explained variance and cumulative explained variance from different components obtained by the rotational component analysis (RC).

	RC-1	RC-2	RC-3	RC-4	RC-5	RC-6	RC-7	RC-8	RC-9
Explained variance (%)	33.8	35.5	14.8	13.6	2.10	0.10	0.10	0.00	0.00
Cumulative proportion (%)	33.8	69.3	84.1	97.7	99.8	99.9	100	100	100

Table R5: Pearson correlations between the logarithm of the cloud properties and the rotational components (RC). Degree of correlation (absolute values): (a) very weak: below 0.2, (b) weak: [0.2, 0.4), (c) moderate: [0.4, 0.6), (d) strong: [0.6, 0.8), and (e) very strong [0.8, 1.0].

Properties	RC-1	RC-2	RC-3	RC-4
CBH	0.969	0.025	−0.001	0.201
CTH	0.919	−0.282	0.076	0.237
Γ_{ad}	−0.896	−0.014	0.073	−0.183
τ	−0.062	−0.971	−0.192	−0.125
Q_{L}	0.036	−0.968	−0.240	0.052
H	0.177	−0.937	0.285	0.094
f_{ad}	−0.010	−0.099	−0.995	−0.025
N_{int}	−0.518	−0.250	−0.244	−0.778
r_{int}	0.382	−0.536	−0.314	0.681

Table R6: Input parameters for the RRTMG model.

Parameter	Value
Cosine of solar zenith angle	0.70
Carbon dioxide concentration	399 ppm
Ultraviolet/Visible surface albedo for direct radiation	0.05
Ultraviolet/Visible surface albedo for diffuse radiation	0.05
Near-infrared surface albedo for direct radiation	0.30
Near-infrared surface albedo for diffuse radiation	0.30

Table R7: Simulated scenarios. For scenarios S1–S3, three individual simulations (sub-cases) have been conducted according to different values for the droplet number concentration.

Scenarios	
Ref.	Double–moment scheme
S1	Single–moment scheme
S2	Vertical homogeneous model
S3	Sub–adiabatic model
S4	Mean vertical N_{d} profile
Sub-cases	a. 220 cm^{-3} b. N_{int} c. 480 cm^{-3}

Table R8: Mean and standard deviation of modeled CREs ($\mathrm{W\,m^{-2}}$) for the SW, LW, and NET (SW + LW) radiation for the reference simulation over all case days. ATM stands for the atmospheric cloud radiative effect defined as the difference between the CREs at the TOA and BOA.

Ref.	$\mathrm{CRE_{SW}}$	$\mathrm{CRE_{LW}}$	$\mathrm{CRE_{NET}}$
TOA	-348.7 ± 78.39	17.51 ± 10.04	-331.2 ± 77.27
ATM	32.94 ± 12.11	-39.16 ± 13.14	-6.225 ± 12.98
BOA	-381.6 ± 86.95	56.66 ± 9.746	-324.9 ± 86.51

Table R9: Mean CRE ($\mathrm{W\,m^{-2}}$) for the SW radiation. Results are given as differences between the new scenario minus the reference simulation (Δ). The root mean square error (RMSE) in $\mathrm{W\,m^{-2}}$ and the Pearson (Pears.) correlation between the new scenarios and the reference simulation are also given.

Scen.	$\mathrm{CRE_{SW,B}}$			$\mathrm{CRE_{SW,T}}$		
	Δ	RMSE	Pears.	Δ	RMSE	Pears.
S1a	−39.2	46.4	0.960	−40.1	47.0	0.952
S1b	−7.04	11.7	0.995	−6.53	11.7	0.994
S1c	−2.59	23.4	0.964	−1.86	24.3	0.951
S2a	−26.1	39.2	0.943	−27.1	39.8	0.930
S2b	7.74	14.2	0.991	8.19	13.6	0.990
S2c	12.9	32.4	0.943	13.7	33.6	0.921
S3a	−31.1	41.4	0.950	−32.9	42.9	0.937
S3b	1.47	10.6	0.993	1.17	10.0	0.992
S3c	6.59	27.7	0.953	6.55	29.0	0.934
S4	−3.13	16.7	0.983	−3.16	17.2	0.977

Table R10: Correlations between the cloud radiative effects for the reference simulation (Ref.) and the cloud properties. For the SW (LW) radiation, results are presented in case of the Spearman (Pearson) correlation.

Properties	$\mathrm{CRE_{SW,B}}$	$\mathrm{CRE_{SW,T}}$	$\mathrm{CRE_{LW,B}}$	$\mathrm{CRE_{LW,T}}$
	Spearman		Pearson	
Q_L	−0.957	−0.955	−0.129	0.181
τ	−0.994	−0.987	0.104	0.148
N_int	−0.471	−0.431	0.428	−0.290
r_int	−0.446	−0.460	−0.395	0.344
CBH	0.148	0.063	−0.389	0.752
CTH	0.143	−0.220	−0.428	0.765
H	−0.795	−0.812	−0.200	0.226
f_ad	−0.284	−0.273	0.145	0.134

Table R11: Mean CRE ($\mathrm{W\,m^{-2}}$) for the LW radiation. Results are given as differences between the new scenario minus the reference simulation (Δ). The root mean square error (RMSE) in $\mathrm{W\,m^{-2}}$ and the Pearson (Pears.) correlation between the new scenarios and the reference simulation are also given.

Scen.	$\mathrm{CRE_{LW,B}}$			$\mathrm{CRE_{LW,T}}$		
	Δ	RMSE	Pears.	Δ	RMSE	Pears.
S1a	−0.11	0.48	0.999	−0.04	0.19	1.000
S1b	−0.05	0.40	0.999	−0.03	0.18	1.000
S1c	−0.01	0.50	0.999	−0.01	0.22	1.000
S2a	0.40	0.79	0.998	0.23	0.51	0.999
S2b	0.51	0.82	0.998	0.27	0.53	0.999
S2c	0.55	0.85	0.998	0.29	0.54	0.999
S3a	−0.05	0.74	0.997	0.33	0.64	0.999
S3b	−0.01	0.73	0.997	0.36	0.65	0.999
S3c	0.02	0.83	0.996	0.37	0.68	0.998
S4	−0.02	0.49	0.999	−0.02	0.22	1.000

References

[1] R. Heinze, A. Dipankar, C. C. Henken, C. Moseley, O. Sourdeval, S. Trömel, X. Xie, P. Adamidis, F. Ament, H. Baars, C. Barthlott, A. Behrendt, U. Blahak, S. Bley, S. Brdar, M. Brueck, S. Crewell, H. Deneke, P. Di Girolamo, R. Evaristo, J. Fischer, C. Frank, P. Friederichs, T. Göcke, K. Gorges, L. Hande, M. Hanke, A. Hansen, H.-C. Hege, C. Hoose, T. Jahns, N. Kalthoff, D. Klocke, S. Kneifel, P. Knippertz, A. Kuhn, T. van Laar, A. Macke, V. Maurer, B. Mayer, C. I. Meyer, S. K. Muppa, R. A. J. Neggers, E. Orlandi, F. Pantillon, B. Pospichal, N. Röber, L. Scheck, A. Seifert, P. Seifert, F. Senf, P. Siligam, C. Simmer, S. Steinke, B. Stevens, K. Wapler, M. Weniger, V. Wulfmeyer, G. Zängl, D. Zhang, and J. Quaas, "Large-eddy simulations over germany using icon: a comprehensive evaluation," *Q. J. R. Meteorol. Soc.*, vol. 143, no. 702, pp. 69–100, 2017.

[2] A. Gassmann and H.-J. Herzog, "Towards a consistent numerical compressible non-hydrostatic model using generalized hamiltonian tools," *Q. J. Roy. Meteor. Soc.*, vol. 134, no. 635, pp. 1597–1613, 2008.

[3] A. Dipankar, B. Stevens, R. Heinze, C. Moseley, G. Zängl, M. Giorgetta, and S. Brdar, "Large eddy simulation using the general circulation model icon," *J. Adv. Model. Earth Syst.*, vol. 7, no. 3, pp. 963–986, 2015.

[4] H. Wan, M. A. Giorgetta, G. Zängl, M. Restelli, D. Majewski, L. Bonaventura, K. Fröhlich, D. Reinert, P. Rípodas, L. Kornblueh, and J. Förstner, "The icon-1.2 hydrostatic atmospheric dynamical core on triangular grids – part 1: Formulation and performance of the baseline version," *Geosci. Model Dev.*, vol. 6, no. 3, pp. 735–763, 2013.

[5] A. Seifert and K. D. Beheng, "A two-moment cloud microphysics parameterization for mixed-phase clouds. part 1: Model description," *Meteorol. Atmos. Phys.*, vol. 92, no. 1, pp. 45–66, 2006.

[6] L. B. Hande, C. Engler, C. Hoose, and I. Tegen, "Parameterizing cloud condensation nuclei concentrations during hope," *Atmos. Chem. Phys.*, vol. 16, no. 18, pp. 12059–12079, 2016.

[7] A. Macke, P. Seifert, H. Baars, C. Barthlott, C. Beekmans, A. Behrendt, B. Bohn, M. Brueck, J. Bühl, S. Crewell, T. Damian, H. Deneke, S. Düsing, A. Foth, P. Di Girolamo, E. Hammann, R. Heinze, A. Hirsikko, J. Kalisch, N. Kalthoff, S. Kinne, M. Kohler, U. Löhnert, B. L. Madhavan, V. Maurer, S. K. Muppa, J. Schween, I. Serikov, H. Siebert, C. Simmer, F. Späth, S. Steinke, K. Träumner, S. Trömel, B. Wehner, A. Wieser, V. Wulfmeyer, and X. Xie, "The hd(cp)^2 observational prototype experiment (hope) – an overview," *Atmos. Chem. Phys.*, vol. 17, no. 7, pp. 4887–4914, 2017.

[8] M. Lebsock and H. Su, "Application of active spaceborne remote sensing for understanding biases between passive cloud water path retrievals," *J. Geophys. Res.-Atmos.*, vol. 119, no. 14, pp. 8962–8979, 2014.

[9] R. Wood and D. L. Hartmann, "Spatial variability of liquid water path in marine low cloud: The importance of mesoscale cellular convection," *J. Climate*, vol. 19, no. 9, pp. 1748–1764, 2006.

[10] R. Wood, "Relationships between optical depth, liquid water path, droplet concentration, and effective radius in adiabatic layer cloud," *University of Washington*, vol. 3, 2006.

[11] V. Ramanathan, R. D. Cess, E. F. Harrison, P. Minnis, B. R. Barkstrom, E. Ahmad, and D. Hartmann, "Cloud-radiative forcing and climate: Results from the earth radiation budget experiment," *Science*, vol. 243, no. 4887, pp. 57–63, 1989.

[12] E. F. Harrison, P. Minnis, B. R. Barkstrom, V. Ramanathan, R. D. Cess, and G. G. Gibson, "Seasonal variation of cloud radiative forcing derived from the earth radiation budget experiment," *J. Geophys. Res.*, vol. 95, no. D11, pp. 18687–18703, 1990.

[13] T. Chen, W. B. Rossow, and Y. Zhang, "Radiative effects of cloud-type variations," *J. Climate*, vol. 13, no. 1, pp. 264–286, 2000.

[14] J. M. Futyan, J. E. Russell, and J. E. Harries, "Cloud radiative forcing in pacific, african, and atlantic tropical convective regions," *J. Climate*, vol. 17, no. 16, pp. 3192–3202, 2004.

[15] N. G. Loeb, B. A. Wielicki, D. R. Doelling, G. L. Smith, D. F. Keyes, S. Kato, N. Manalo-Smith, and T. Wong, "Toward optimal closure of the earth's top-of-atmosphere radiation budget," *J. Climate*, vol. 22, no. 3, pp. 748–766, 2009.

[16] B. Lin, P. Minnis, T.-F. Fan, Y. Hu, and W. Sun, "Radiation characteristics of low and high clouds in different oceanic regions observed by ceres and modis," *Int. J. Remote Sens.*, vol. 31, no. 24, pp. 6473–6492, 2010.